Stability Theory for a Pair of Trailing Vortices

S. C. CROW*
The Boeing Company, Seattle, Wash.

Trailing vortices do not decay by simple diffusion. Usually they undergo a symmetric and nearly sinusoidal instability, until eventually they join at intervals to form a train of vortex rings. The present theory accounts for the instability during the early stages of its growth. The vortices are idealized as interacting lines; their core diameters are taken into account by a cutoff in the line integral representing self-induction. The equation relating induced velocity to vortex displacement gives rise to an eigenvalue problem for the growth rate of sinusoidal perturbations. Stability is found to depend on the products of vortex separation b and cutoff distance d times the perturbation wavenumber. Depending on those products, both symmetric and antisymmetric eigenmodes can be unstable, but only the symmetric mode involves strongly interacting long waves. An argument is presented that $d/b = 0.063$ for the vortices trailing from an elliptically loaded wing. In that case, the maximally unstable long wave has a length $8.6b$ and grows by a factor e in a time $9.4(A_R/C_L)(b/V_o)$, where A_R is the aspect ratio, C_L is the lift coefficient, and V_o is the speed of the aircraft. The vortex displacements are symmetric and are confined to fixed planes inclined at 48° to the horizontal.

Nomenclature

a = rate of displacement amplification
A_R = aspect ratio of wing
b = separation between vortices
c = vortex core diameter
C_L = lift coefficient
d = cutoff distance in self-induction integral, proportional to c
D = diameter of vortex ring
$\mathbf{e}_x$ = longitudinal unit vector
$\mathbf{e}_y$ = lateral unit vector
$\mathbf{e}_z$ = vertical unit vector
k = perturbation wavenumber
$d\mathbf{L}$ = line increment directed along vortex
$\mathbf{r}$ = radial vortex displacement, with components (y,z)
$\hat{\mathbf{r}}$ = displacement eigenvector, with components $(\hat{y},\hat{z})$
$\mathbf{R}$ = separation between points on vortices
s = position of an unperturbed vortex along $\mathbf{e}_y$-axis
t = time
$\mathbf{u}$ = perturbation velocity at vortex, with components (u,v,w)
$\mathbf{U}$ = total induced velocity, $\mathbf{u} - \mathbf{e}_z(\Gamma_o/2\pi b)$
V_o = aircraft speed
x = coordinate along unperturbed vortex
α = dimensionless amplification rate, $(2\pi b^2/\Gamma_o)a$
β = dimensionless wavenumber, kb
Γ = circulation around a vortex, positive or negative
Γ_o = magnitude of circulation $|\Gamma|$
δ = dimensionless cutoff distance, kd
θ = angle of $\hat{\mathbf{r}}$ from the horizontal
ν = kinematic viscosity
$\chi(\beta)$ = first mutual-induction function, $\int_0^\infty \frac{\cos\beta\xi}{(\xi^2+1)^{3/2}}\,d\xi$
$\psi(\beta)$ = second mutual-induction function, $\int_0^\infty \frac{\cos\beta\xi + \beta\xi\sin\beta\xi}{(\xi^2+1)^{3/2}}\,d\xi$
$\omega(\delta)$ = self-induction function, $\int_\delta^\infty \frac{\cos\xi + \xi\sin\xi - 1}{\xi^3}\,d\xi$

Subscripts

1 = portside trailing vortex
2 = starboard trailing vortex
A = antisymmetric eigenmode
S = symmetric eigenmode
m = vortex inducing a field
n = vortex acted upon by that field
max = maximally amplified mode

1. Introduction

THE power of an aircraft is spent in generating its wake. Not all the power is lost at once to friction. A good part of it, the part corresponding to induced drag, concentrates into a pair of contra-rotating vortices that trail behind the aircraft. The coherent, energetic flow around the trailing vortices of a heavy airliner poses a threat to lightplanes, and it is important to know how long the danger persists.

Trailing vortices form out of the vortex sheet leaving the trailing edge of a wing. The way the sheet wraps into a pair of contra-rotating vortices is well understood.[1] The vortices persist for a relatively long time, a minute or two, but not nearly so long as would be the case if they simply diffused into one another. Sometimes moisture condenses in their cores so that their motion becomes visible, and then the trailing vortices are seen to undergo a slow, symmetric, and nearly sinusoidal instability. Figure 1 is a photograph of such an occurrence, reproduced here through the courtesy of Meteorology Research Inc.[2] The vortex cores recede and draw together in a wavy pattern, until they connect at the nearer points to form a train of vortex rings.

Once the rings have formed, the wake quickly disintegrates into a harmless turbulent state. The persistence of coherent flow depends mainly on the growth rate of the instability that precedes the formation of vortex rings. The object of this study is to find the cause of the instability and its growth rate.

Scorer[3] has proposed buoyancy as the cause, though no quantitative theory has arisen around the idea. Trailing vortices induct each other downward and carry a column of recirculating air down with them. If the atmosphere is stably stratified, the descending column is warmer than its surroundings and might buoy upward as a wave. Certainly buoyancy could stop the descent of the vortex pair.

The analysis presented here is based on a more elementary model: the wake is idealized as a pair of nearly parallel vor-

Presented as Paper 70-53 at the AIAA 8th Aerospace Sciences Meeting, New York, January 19–21, 1970; submitted December 22, 1969, revision received April 6, 1970. I began this work during the spring of 1963, as a consulting project for P. B. MacCready of Meteorology Research Inc., Altadena, Calif. I profited greatly at that time from conversations with him and with P. B. S. Lissaman at the California Institute of Technology. The results of that early work have so far been available only in manuscript form. Because of rising interest in the behavior of trailing vortices, I have refined and completed the theory of their instability, and the work appears here for the first time as a formal paper.

* Staff Scientist, Boeing Scientific Research Laboratories. Member AIAA.

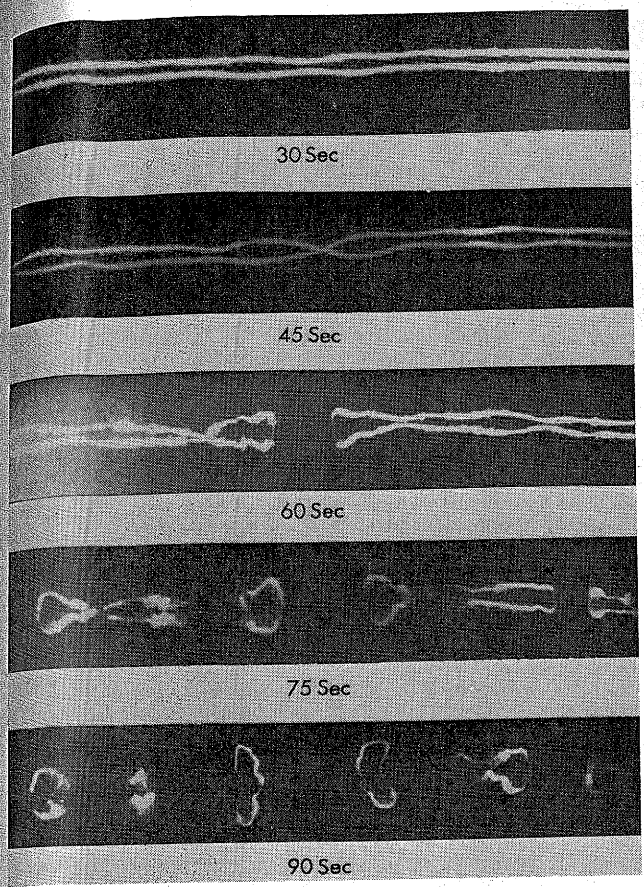

Fig. 1 Vortex trail of a B-47, photographed with a camera aimed straight upwards. The time elapsed since the passage of the aircraft appears under each picture.

tex lines interacting in neutrally stable air. The vortices are convected in their own induced field. Gusts or flight-path irregularities displace the two lines slightly in a random fashion, and the displacements amplify under mutual induction. The wavy pattern seen in practice is the most rapidly growing mode of instability. The model appears fully capable of explaining the observations, so buoyancy is probably not an essential mechanism.

2. Convection in the Induced Field

The analysis begins with the kinematic relation[4] between vorticity and velocity in an incompressible fluid:

$$\mathbf{U}_n = \sum_{m=1}^{2} \Gamma_m \int \frac{\mathbf{R}_{mn} \times d\mathbf{L}_m}{4\pi|\mathbf{R}_{mn}|^3} \tag{1}$$

where n takes on the values 1 and 2. Equation (1) gives the velocity at a point on the nth vortex in terms of the relative position $\mathbf{R}_{mn}$, length $d\mathbf{L}_m$, and strength Γ_m of all the vortex elements in the flow. Some of the geometrical quantities are illustrated in Fig. 2. The vector distance from an element of vortex n to another of vortex m satisfies

$$\mathbf{R}_{mn} = \mathbf{e}_x(x_m' - x_n) + \mathbf{e}_y(s_m - s_n) + (\mathbf{r}_m' - \mathbf{r}_n) \tag{2}$$

where the first two terms on the right involve the locations of the unperturbed vortices, and the third represents radial displacement from their nominal positions. The primes are used to distinguish points lying on the same vortex, in case $m = n$. The displacement $\mathbf{r}_n$ has components in the lateral and vertical directions and is a function of x_n and t: $\mathbf{r}_n = \mathbf{e}_y y_n(x_n,t) + \mathbf{e}_z z_n(x_n,t)$. The relation between $d\mathbf{L}_n$ and a displacement dx_n in the $\mathbf{e}_x$-direction is apparent from the detail sketch of Fig. 3:

$$d\mathbf{L}_n = (\mathbf{e}_x + \partial\mathbf{r}_n/\partial x_n)dx_n \tag{3}$$

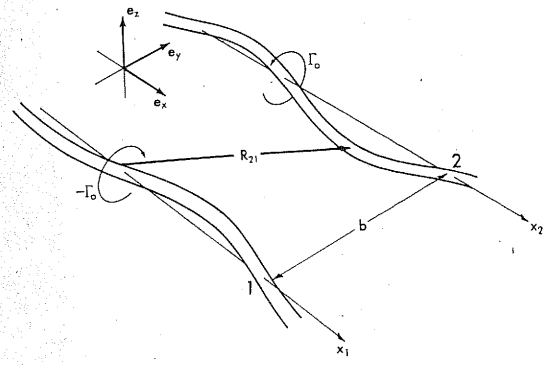

Fig. 2 Geometrical quantities entering the analysis. The vortices are viewed from above, so the aircraft generating them lies beyond the upper left-hand corner of the figure.

The circulations Γ_n and lateral locations s_n are related to the quantities shown in Fig. 2 as follows: $\Gamma_1 = -\Gamma_o$, $\Gamma_2 = +\Gamma_o$; $s_1 = -b/s$, $s_2 = +b/2$. In the absence of perturbations, the vortices drift downward at a rate $\Gamma_o/2\pi b$, so the coordinates of Figs. 2 and 3 must be envisaged as moving downward at that rate as well.

The only dynamics implied in Eq. (1) is the circulation theorem, which enabled Γ_m to be removed from the integral as a constant. The vorticity-transport theorem closes the dynamical problem: in an inviscid and neutrally buoyant fluid, elements of a vortex line move with fluid particles. In mathematical terms,

$$\partial\mathbf{r}_n/\partial t + u_n(\partial\mathbf{r}_n/\partial x_n) = \mathbf{e}_y v_n + \mathbf{e}_z w_n \tag{4}$$

where (u_n,v_n,w_n) are the components of $\mathbf{U}_n + \mathbf{e}_z(\Gamma_o/2\pi b)$, which is the velocity of convection with respect to the downward moving coordinates. Equations (1–4) thus provide a self-contained description of the vortices as they evolve in their induced field.

It is necessary to depart from the notion of vortex lines to a certain extent, however, in order to account properly for the self-induction of a vortex. Otherwise a difficulty arises with the $m = n$ term on the right of Eq. (1): the line integral diverges logarithmically around $|\mathbf{R}_{nn}| = 0$. The divergence is artificial, because the vortices actually have finite core diameters as shown in the figures. Elements of a vortex lying within a core diameter of each other cannot be idealized as interacting lines. Some means must be provided to relax the singularity in the self-induction integral, and the means adopted here is to cut the integral off an arc-length d on either side of the point $|\mathbf{R}_{nn}| = 0$. Rosenhead[5] and Hama[6] have used similar artifices to account for self-induction in other contexts. The cutoff distance d is taken as proportional to the diameter c of the vortex cores. The constant of proportionality is calculated approximately in Sec. 6, where the cutoff method is applied to two problems whose solutions by other means are known.

The system of Eqs. (1–4), together with the cutoff method for evaluating self-induction, is a model of the phenomenon shown in Fig. 1 rather than an exact theory. The model is probably as sound as the notion of compact trailing vortices itself, and it has the advantage of suppressing irrelevant complications that would arise in an exact theory, like surface

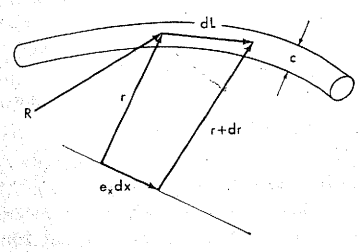

Fig. 3 Relation between an arc-length dL and a displacement $e_x dx$ down the longitudinal axis.

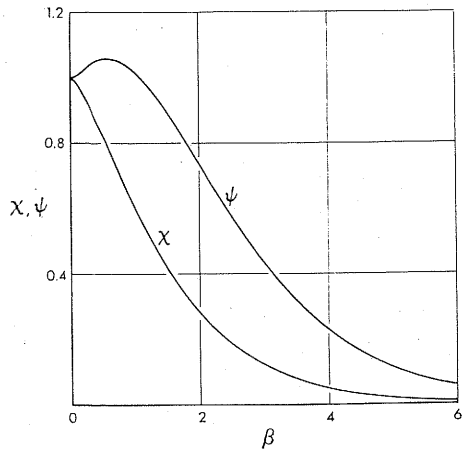

Fig. 4 Mutual-induction functions.

ripples on the vortex cores.[7] Like any model, however, it has a limited domain of validity. Equations (1–4) cannot apply to vortices so thick that d is comparable to b, and they may not apply to displacement perturbations having a wavelength as short as d. The model predicts the instability that actually occurs, but it also predicts spurious instabilities that lie outside its domain of physical validity. No trouble arises, as long as common sense is used to distinguish the physical instability from purely mathematical ones incidental to the introduction of cutoff integrals.

3. Linearized Eigenvalue Problem

The next step is to suppose that the vortices are displaced only slightly from their unperturbed positions. The problem posed in Eqs. (1–4) can be linearized, as long as the vortex displacements remain small compared with b and their slopes remain small compared with 1: $|\mathbf{r}_n|/b \ll 1$ and $|\partial \mathbf{r}_n/\partial x_n| \ll 1$. The first inequality means that the third term on the right of Eq. (2) is generally small compared with the others. The second inequality means that the second term in the brackets of Eq. (3) is much smaller in magnitude than the first. To first order in the perturbation quantities $|\mathbf{r}_n|/b$ and $|\partial \mathbf{r}_n/\partial x_n|$, Eq. (1) assumes the form

$$\mathbf{U}_n = \sum_{m=1}^{2} \frac{\Gamma_m}{4\pi} \left\{ -\mathbf{e}_z \int_{-\infty}^{\infty} \frac{(s_m - s_n)dx_m'}{[(x_m' - x_n)^2 + (s_m - s_n)^2]^{3/2}} + \mathbf{e}_x \int_{-\infty}^{\infty} \frac{(s_m - s_n)(\partial z_m'/\partial x_m')dx_m'}{[(x_m' - x_n)^2 + (s_m - s_n)^2]^{3/2}} + \mathbf{e}_y \int_{-\infty}^{\infty} \frac{[(z_m' - z_n) - (x_m' - x_n)(\partial z_m'/\partial x_m')]}{[(x_m' - x_n)^2 + (s_m - s_n)^2]^{3/2}} dx_m' + \mathbf{e}_z \int_{-\infty}^{\infty} \left(\frac{3(s_m - s_n)^2(y_m' - y_n)}{[(x_m' - x_n)^2 + (s_m - s_n)^2]^{5/2}} - \frac{[(y_m' - y_n) - (x_m' - x_n)(\partial y_m'/\partial x_m')]}{[(x_m' - x_n)^2 + (s_m - s_n)^2]^{3/2}} \right) dx_m' \right\} \quad (5)$$

where cutoffs in the integrals for $m = n$ are understood. Note that it has *not* been necessary to assume that $|\mathbf{r}_n|/c \ll 1$, a restriction that might arise if the displacements were treated as shear waves in the vortex cores (cf. Ref. 7). The present model requires a less severe linearization than an expansion of the primitive equations of motion would have done.

The first term on the right of Eq. (5) involves no perturbation quantities and represents downward induction at the rate $\Gamma_o/2\pi b$, as is easily verified by direct integration. The second term represents longitudinal convection and enters the dynamics through the term $u_n \partial \mathbf{r}_n/\partial x_n$ in Eq. (4). Longitudinal convection is a second-order effect, however, and drops out when Eq. (4) itself is linearized. The third and fourth terms on the right of Eq. (5) are first-order approximations of the velocity components v_n and w_n, which are the dominant convection terms in Eq. (4). The linearized version of Eq. (4) is then as follows:

$$\frac{\partial \mathbf{r}_n}{\partial t} = \sum_{m=1}^{2} \frac{\Gamma_m}{4\pi} \times \left\{ \mathbf{e}_y \int_{-\infty}^{\infty} \frac{[(z_m' - z_n) - (x_m' - x_n)(\partial z_m'/\partial x_m')]}{[(x_m' - x_n)^2 + (s_m - s_n)^2]^{3/2}} dx_m' + \mathbf{e}_z \int_{-\infty}^{\infty} \left(\frac{3(s_m - s_n)^2(y_m' - y_n)}{[(x_m' - x_n)^2 + (s_m - s_n)^2]^{5/2}} - \frac{[(y_m' - y_n) - (x_m' - x_n)(\partial y_m'/\partial x_m')]}{[(x_m' - x_n)^2 + (s_m - s_n)^2]^{3/2}} \right) dx_m' \right\} \quad (6)$$

Equation (6) admits solutions of exponential form, namely $\mathbf{r}_n(x_n,t) = \hat{\mathbf{r}}_n e^{at+ikx_n}$. No generality is lost in considering such solutions, since an arbitrary function can be synthesized from them by Fourier integration. As a result of the assumed exponential form of solution, Eq. (6) changes from an integro-differential equation into a set of algebraic equations for the constant vectors $\hat{\mathbf{r}}_n$:

$$a\hat{y}_1 = -\frac{\Gamma_2}{2\pi} \hat{z}_1 \int_0^{\infty} \frac{dx}{(x^2 + b^2)^{3/2}} + \frac{\Gamma_2}{2\pi} \hat{z}_2 \int_0^{\infty} \frac{\cos kx + kx \sin kx}{(x^2 + b^2)^{3/2}} dx + \frac{\Gamma_1}{2\pi} \hat{z}_1 \int_d^{\infty} \frac{\cos kx + kx \sin kx - 1}{x^3} dx \quad (7a)$$

$$a\hat{z}_1 = -\frac{\Gamma_2}{2\pi} \hat{y}_1 \int_0^{\infty} \frac{dx}{(x^2 + b^2)^{3/2}} + \frac{\Gamma_2}{2\pi} \hat{y}_2 \int_0^{\infty} \frac{\cos kx}{(x^2 + b^2)^{3/2}} dx - \frac{\Gamma_1}{2\pi} \hat{y}_1 \int_d^{\infty} \frac{\cos kx + kx \sin kx - 1}{x^3} dx \quad (7b)$$

together with a complementary pair of equations obtained by transposing the subscripts 1 and 2. The dummy variable x has replaced the quantity $(x_m' - x_n)$ appearing in Eq. (6), and a partial integration has simplified the second member of Eqs. (7). The cutoff length d appears here explicitly for the first time. Equations (7) have eigenvector solutions $\hat{\mathbf{r}}_n$ only for certain eigenvalues of a, which happen to be either purely imaginary or purely real. Imaginary values correspond to neutrally stable oscillations of the vortex pair. Real and positive values of a are the amplification rates of exponentially growing instabilities.

It is convenient to rewrite Eqs. (7) and their complements in terms of dimensionless quantities, represented by the lower case Greek characters defined in the nomenclature list:

$$\alpha\hat{y}_1 = -\hat{z}_1 + \psi\hat{z}_2 - \beta^2\omega\hat{z}_1 \quad (8a)$$

$$\alpha\hat{z}_1 = -\hat{y}_1 + \chi\hat{y}_2 + \beta^2\omega\hat{y}_1 \quad (8b)$$

$$\alpha\hat{y}_2 = \hat{z}_2 - \psi\hat{z}_1 + \beta^2\omega\hat{z}_2 \quad (8c)$$

$$\alpha\hat{z}_2 = \hat{y}_2 - \chi\hat{y}_1 - \beta^2\omega\hat{y}_2 \quad (8d)$$

The dimensionless interaction functions $\chi(\beta)$, $\psi(\beta)$, and $\omega(\delta)$ come from the trigonometric integrals in Eqs. (7) and can be evaluated analytically as follows:

$$\chi(\beta) = \beta K_1(\beta), \quad \psi(\beta) = \beta^2 K_0(\beta) + \beta K_1(\beta)$$

$$\omega(\delta) = \tfrac{1}{2}[(\cos\delta - 1)/\delta^2 + \sin\delta/\delta - Ci(\delta)]$$

$Ci(\delta)$ is the integral cosine,[8] and $K_0(\beta)$ and $K_1(\beta)$ are modified Bessel functions of the second kind.[9] The mutual-induction functions $\chi(\beta)$ and $\psi(\beta)$ are plotted in Fig. 4, and the self-induction function $\omega(\delta)$ is plotted on semi-logarithmic coor-

dinates in Fig. 5. α is an eigenvalue of Eqs. (8) and is related to β and δ through the interaction functions. Whether a is real or imaginary thus depends entirely upon the dimensionless wavenumber β and cutoff δ, since $a(k,b,d,\Gamma_o) = (\Gamma_o/2\pi b^2)\alpha(\beta,\delta)$, a result that could have been anticipated from dimensional considerations.

Equations (8) have been arranged in four columns, each of which has a distinct physical meaning. The column on the left of the equality signs represents the rate of change of the displacement amplitudes in time. The first column on the right represents the zeroth-order field of one vortex acting on the displacement perturbations of the other. The potential field of vortex 1, for example, combined with the general downward motion of the vortex pair, results in a two-dimensional field of pure strain in the vicinity of vortex 2. Displacement perturbations of vortex 2 tend to diverge under the strain. If only the first column on the right of Eqs. (8) were effective, then α would be ± 1, and the positive root would correspond to unconditional instability. The second column on the right represents the velocity perturbations at one vortex due to the displacement perturbations of the other. The velocity perturbations can retard or accelerate instability, depending on the value of the dimensionless wavenumber β.

The third column on the right of Eqs. (8) represents self-induction. If self-induction alone were effective, then α would be $\pm i\beta^2\omega(\delta)$, and the vortices would execute neutrally stable oscillations independently of each other. The third column indeed must dominate the others for very slender vortices, since $\omega(\delta)$ grows as $\log(1/\delta)$ when δ becomes small, as is evident from Fig. 5. The nature of the oscillation depends on the phase difference between the eigenvectors $\hat{\mathbf{r}}_n$ associated with the two roots $\alpha = \pm i\beta^2\omega(\delta)$. If the net values of $\hat{y}_n$ and z_n differ by a factor i, then the nth vortex is bent into a helix, and the helix travels along the $\mathbf{e}_x$-axis with a phase velocity $(\Gamma_o k/2\pi)\omega(\delta)$. If $\hat{y}_n$ and $\hat{z}_n$ are in phase, on the other hand, then the vortex remains confined to a plane, which spins at an angular frequency $(\Gamma_o k^2/2\pi)\omega(\delta)$, in a direction *opposite* the general rotation around the vortex. In either event, self-induction tends to stabilize the vortex pair. If δ is sufficiently small, then displacement perturbations of a given β uncouple, and each vortex spins independently under its own induction. At larger values of δ, perturbations interlock from one vortex to the other and diverge.

4. Symmetric and Antisymmetric Modes

A sinusoidally perturbed vortex pair has four degrees of freedom, so the eigenvalue $\alpha(\beta,\delta)$ has four roots. The roots could be found by a straightforward solution of the determinant associated with Eqs. (8). As with most physical problems, however, it is more revealing to combine the eigenvectors into independent modes, each involving fewer degrees of freedom than the system as a whole. The independent modes of a vortex pair are as follows:

$$\begin{aligned} \hat{y}_S &= \hat{y}_2 - \hat{y}_1,\ z_S = \hat{z}_2 + \hat{z}_1 \\ \hat{y}_A &= \hat{y}_2 + \hat{y}_1,\ \hat{z}_A = \hat{z}_2 - \hat{z}_1 \end{aligned} \tag{9}$$

If mode S alone were excited, then the vortex distortions would appear symmetric to an observer on the ground. If mode A alone were excited, then the distortions would appear antisymmetric. In that sense, the subscripts S and A denote symmetric and antisymmetric modes.

Independent pairs of equations for the two modes follow from Eqs. (8) and (9):

$$\begin{aligned} \alpha\hat{y}_S &= (1 - \psi + \beta^2\omega)\hat{z}_S,\ \alpha\hat{z}_S = (1 + \chi - \beta^2\omega)\hat{y}_S \\ \alpha\hat{y}_A &= (1 + \psi + \beta^2\omega)\hat{z}_A,\ \alpha\hat{z}_A = (1 - \chi - \beta^2\omega)\hat{y}_A \end{aligned} \tag{10}$$

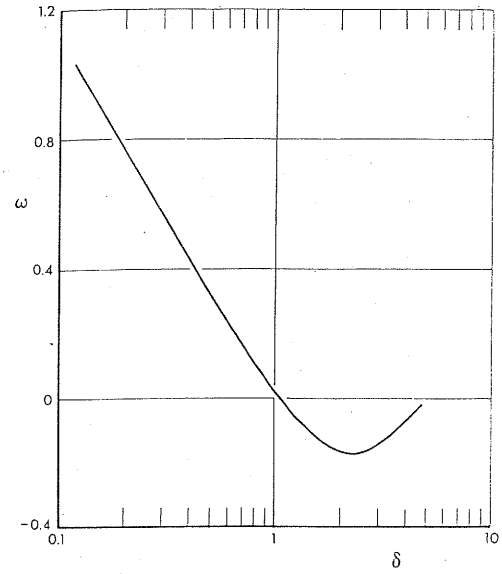

Fig. 5 Self-induction function plotted on semi-logarithmic coordinates.

The four roots of α are thus $\pm\alpha_S$ and $\pm\alpha_A$, where

$$\begin{aligned} \alpha_S &= [(1 - \psi + \beta^2\omega)(1 + \chi - \beta^2\omega)]^{1/2} \\ \alpha_A &= [(1 + \psi + \beta^2\omega)(1 - \chi - \beta^2\omega)]^{1/2} \end{aligned} \tag{11}$$

the principal square-root being intended in either case. When the two factors inside the brackets of one of Eqs. (11) have the same sign, the corresponding α is real, and the mode is unstable. Otherwise the mode is a neutrally stable oscillation, qualitatively similar to the oscillation of an isolated vortex. The vortices are twisted into travelling helices or are confined to spinning planes, depending on the phase difference between the $\hat{\mathbf{r}}_n$ corresponding to the imaginary eigenvalues $\pm\alpha$.

Figure 6 is a stability diagram for mode S based on the first of Eqs. (11), and Fig. 7 is the diagram for mode A. The eigenvalues are real in the shaded regions, which therefore are regions of instability. δ/β is used as the abscissa instead of δ, because δ/β equals d/b, a geometrical property of the vortices independent of the wavenumber k. The stability diagrams span the interval $0 \leq \delta/\beta \leq 1$, and they could have been extended to even larger values. When $\delta/\beta = 1$, however, the separation b of the vortices is little more than twice their core

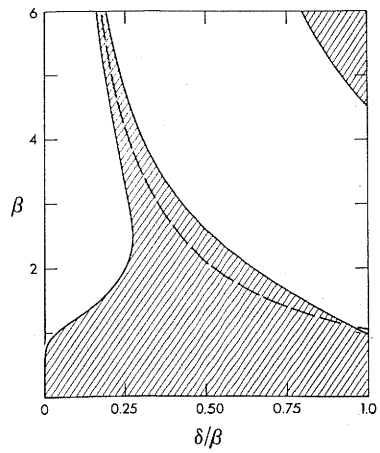

Fig. 6 Stability diagram for mode S. Regions of instability are shaded, and the locus of vanishing self-induction is shown as a dashed line. The shaded region in the upper right-hand corner is probably a spurious effect of the cut-off model.

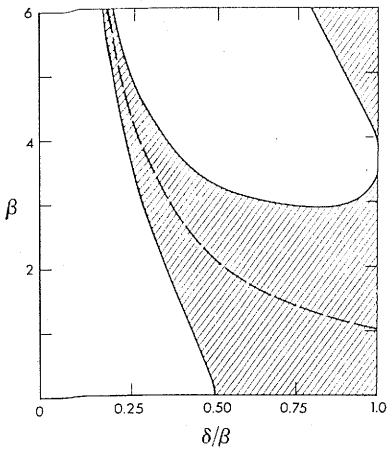

Fig. 7 Stability diagram for mode *A*.

diameters c (cf. Sec. 6), so larger values of δ/β are physically meaningless.

Outside the shaded regions of the diagrams, the tendency of the vortices to spin in their own fields overcomes their mutual induction, and the pair is stable. The tendency to spin diminishes as d grows to a significant fraction of the perturbation wavelength $2\pi/k$. The dashed curves in Figs. 6 and 7 represent the locus of $\delta = 1.06$, corresponding to a value of 0.17 for the ratio of cutoff distance over wavelength. According to Fig. 5, the tendency to spin vanishes altogether at $\delta = 1.06$. Almost any interaction between the two vortices leads to instability, as is evident from the diagrams. The regions well above and to the right of the dashed lines involve vortices that are rather thick compared with the perturbation wavelength. The cutoff model may not portray those regions accurately.

Once the vortices become unstable, the eigenmode associated with the positive root of α quickly dominates the decaying mode of the negative root. The growing perturbations are planar standing waves, as sketched in Fig. 8. The upper drawing shows the vortices when mode S alone is excited, and the decaying part of the disturbance has died away. The lower drawing shows the vortices deforming in mode A. The planes are fixed at angles $\theta(\beta,\delta)$ to the horizontal, where $\tan\theta = \hat{z}_2/\hat{y}_2$. Expressions for the planar angles of modes S and A follow from Eqs. (9–11):

$$\tan\theta_S = [(1 + \chi - \beta^2\omega)/(1 - \psi + \beta^2\omega)]^{1/2}$$
$$\tan\theta_A = [(1 - \chi - \beta^2\omega)/(1 + \psi + \beta^2\omega)]^{1/2} \qquad (12)$$

5. Maximum Amplification Rates

Upstream conditions determine the ratio δ/β, so the instabilities of a given vortex pair lie on a vertical cut through the $(\beta,\delta/\beta)$-plane of Figs. 6 and 7. For each δ/β, perturbations spanning a whole spectrum of wavenumbers β can be unstable, and the question arises whether any particular β ultimately dominates. If atmospheric turbulence excited all wavenumbers equally, then the mode having the maximum α for a given δ/β would become the dominant instability. Turbulence does not excite uniformly across the wavenumber spectrum, but for now it suffices to concentrate on modes that have *local* maxima of α above a given δ/β. The way turbulence imposes a final selection among those preferred modes is discussed in Sec. 7.

Figure 9 shows profiles of α along three vertical cuts through the $(\beta,\delta/\beta)$-plane. The solid curves represent α_S and the dotted α_A. The curves were computed from Eqs. (11) with the aid of the table of integral cosines in Ref. 8 and the tables of Bessel functions in Ref. 9. Only real eigenvalues are displayed; the gaps along the β-axis lie in the unshaded regions of Figs. 6 and 7. The upper plot applies to vortices having $\delta/\beta = 0.2$, the middle to $\delta/\beta = 0.3$, and the lower to $\delta/\beta = 0.4$. None of those values is as small as the δ/β of an aircraft wake, which is found in Sec. 6 to be about 0.063. The three cuts in Fig. 9 were chosen to illustrate the point that α_S is real in two separate regions and has two local maxima whenever $\delta/\beta \lesssim 0.4$. α_A has only one maximum along the β-axis for any reasonable value of δ/β.

Considering the middle plot of Fig. 9, as an example, one can see that α_S has maxima at $\beta = 1.2$ and 3.4, and that α_A has a maximum at $\beta = 3.6$. Wavenumbers β_{max} associated with maximum amplification rates can be found in a similar way for each δ/β, and the results are plotted in Fig. 10. The solid and dashed lines refer to mode S and the dotted line to mode A. Low-wavenumber peaks of α_S, such as the one at $\beta = 1.2$ in the middle plot of Fig. 9, fall along the solid curve in Fig. 10. Those peaks correspond to waves whose lengths greatly exceed the vortex core diameters. The long waves interact strongly, and the stabilizing effect of self-induction is strong as well. The remaining peaks of α_S lie along the dashed curve of Fig. 10, and the peaks of α_A lie along the dotted curve. The dashed and dotted curves are not far from the locus of $\delta = 1.06$, where self-induction vanishes. They therefore represent weak interactions, weakly resisted by self-induction. Only the symmetric mode S can be unstable in spite of strong self-induction.

The maximum amplification rates themselves are plotted against δ/β in Fig. 11. The three types of curve have the same meaning as in Fig. 10: the solid line represents strong interactions in the symmetric mode, the dashed line represents weak interactions in the symmetric mode, and the dotted line represents weak interactions in the antisymmetric mode. At $\delta/\beta = 0.3$, for example, the α_{max} of mode S under strong interaction is 0.77, as can be seen directly from Fig. 9. Note that strong interactions do not give rise to modes growing more rapidly than those involving weak interactions; the strong mutual induction and strong self-induction roughly balance. α_{max} is not far from unity in the interval $0 \leq \delta/\beta \leq 0.4$ for all three kinds of interaction.

For each δ/β and associated β_{max}, the tangent of the planar angle θ_{max} can be calculated from Eqs. (12). Those tangents are plotted in Fig. 12, in which the curves have the usual meanings. Throughout the interval $0 \leq \delta/\beta \lesssim 0.4$, the planes containing any maximally unstable mode are inclined at about 45° to the horizontal. The three quantities α_{max}, β_{max}, and θ_{max} completely describe the instability, and all that remains is to choose a value of δ/β at which to evaluate them.

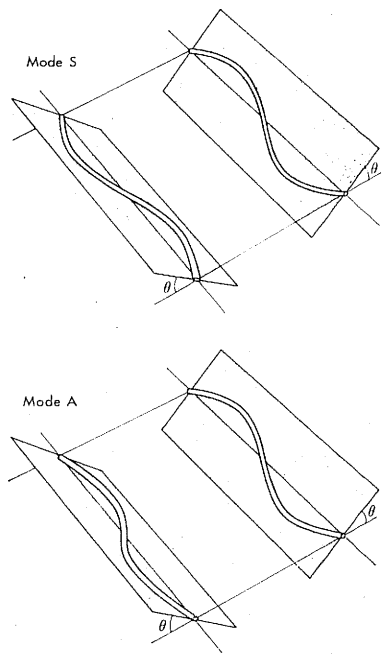

Fig. 8 Shapes of unstable modes after transients have died away.

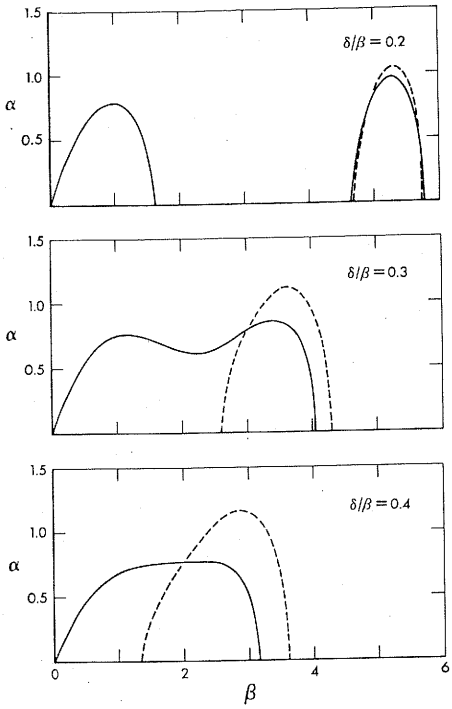

Fig. 9 Amplification rates along three vertical cuts through the $(\beta,\delta/\beta)$-plane of Figs. 6 and 7. The solid line denotes mode S and the dotted line mode A.

6. Selection of a Cutoff Distance

Suppose that a diameter c of the vortex cores is defined in terms of the distribution of vorticity within them. δ/β can then be written as a product of (c/b) and (d/c). The factor (c/b) is a physical quantity, having nothing to do with the mathematical model being used for this stability analysis. (c/b) depends on the lift distribution over the wing generating the vortices and must be calculated aerodynamically. The remaining factor (d/c) depends on the relation of the cutoff model to exact dynamics. The only way to determine (d/c) is to apply the cutoff method to a problem whose exact solution is known a priori.

The two factors should be calculated on the basis of a common assumption about the core structure. The assumption adopted here is that vorticity is distributed uniformly within cores of diameter c and is zero outside, so the cores rotate like solid bodies. For a uniform vorticity distribution, both (c/b) and (d/c) can be drawn from past work.

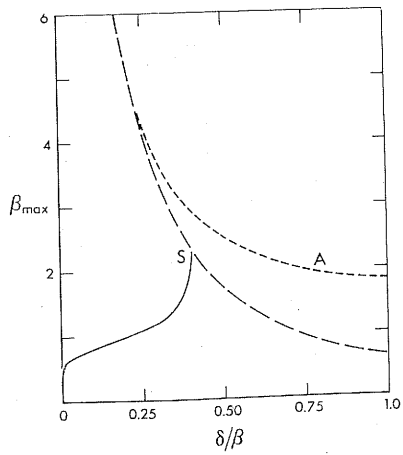

Fig. 10 Wavenumbers β at which maximum amplification occurs for fixed δ/β. The solid line denotes strongly interacting long waves of mode S, the dashed line denotes short waves of mode S, and the dotted line denotes mode A.

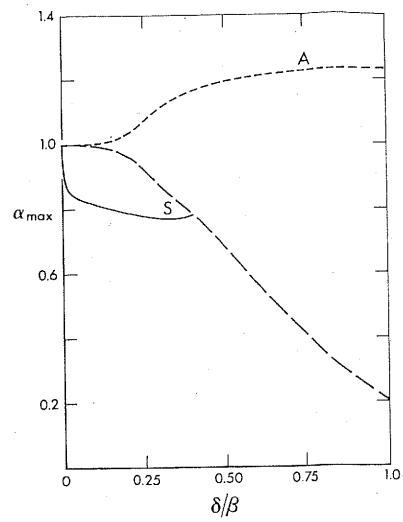

Fig. 11 Maximum amplification rates. The three kinds of line have the same meanings as in Fig. 10.

Spreiter and Sacks (Ref. 1) estimate that $(c/b) = 0.197$ behind an elliptically loaded wing. They assume that energy is conserved as a vortex sheet wraps into two distinct vortices in solid-body rotation. Conservation of energy is not strictly consistent with eventual solid-body rotation, since dissipation is required to smooth the layered vorticity of a rolled-up sheet. Nevertheless, the estimate $(c/b) = 0.197$ is probably accurate enough and is certainly a reliable lower bound for the assumed wing loading and vorticity distribution.

The factor (d/c) is to be found by applying the cutoff method to a problem having a known solution and involving a vortex core in solid-body rotation. Fortunately, there are two such problems, or rather two limiting cases, both due to Kelvin (Sir W. Thomson).

The first problem concerns a displacement wave travelling around a columnar vortex. Kelvin showed in Ref. 7 that a very long wave ($kc \ll 1$) rotates around the vortex at an angular frequency

$$(\Gamma_o/4\pi)k^2[\log(1/kc) + 1.0590]$$

in a direction opposite the circulatory flow. It was argued in Sec. 3 on the basis of the cutoff model that a wave on an isolated vortex spins at an angular frequency $(\Gamma_o k^2/2\pi)\omega(\delta)$ in the retrograde direction. The angular frequency for very long waves ($\delta = kd \ll 1$) is

$$(\Gamma_o/4\pi)k^2[\log(1/kd) - 0.0772]$$

where the limiting form for the integral cosine appearing in $\omega(\delta)$ has been taken from Ref. 8. The cutoff model agrees with Kelvin's theory, provided

$$(d/c) = 0.3210 \tag{13}$$

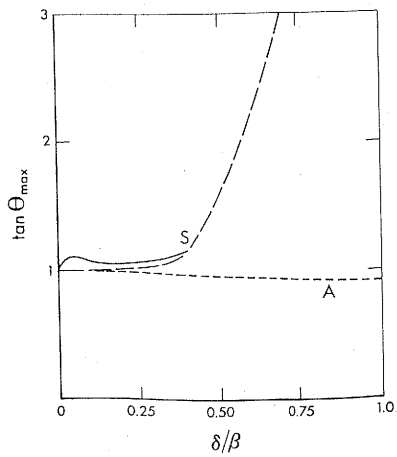

Fig. 12 Planar angles at maximum amplification. The three kinds of line have the same meanings as in Fig. 10.

The second problem concerns the speed of a vortex ring.[10] Using some fundamental theorems about vorticity, Kelvin found that a vortex ring of diameter D propagates at a speed

$$(\Gamma_o/2\pi D)[\log(D/c) + 1.8294] \tag{14}$$

if the ring is slender ($c/D \ll 1$). According to the cutoff model, the speed of a vortex ring is exactly

$$(\Gamma_o/2\pi D)\log[1/\tan(d/2D)]$$

and the limit appropriate for comparison with Kelvin's result is

$$(\Gamma_o/2\pi D)[\log(D/d) + 0.6931]$$

The cutoff model again agrees with Kelvin's theory, provided

$$(d/c) = 0.3210 \tag{15}$$

exactly the same as Eq. (13).

Equations (13) and (15) pertain to radically different flows, yet the two estimates of (d/c) are the same. The coincidence suggests that the cutoff model becomes asymptotically exact in the limit of small core diameter, provided that the cutoff length d is chosen as $0.321c$. If so, then the model could prove enormously useful for machine computation of vortex motions. †

Combined with the estimate $(c/b) = 0.197$ of Spreiter and Sacks, Eq. (13) or (15) implies that $\delta/\beta = 0.063$ behind an elliptically loaded wing. It must be remembered that δ/β has been calculated on the basis of a particular assumption about the structure of the vortex cores, namely that their vorticity is distributed uniformly. There are other possibilities, for example the bell-shaped distribution of a vortex diffusing under the action of viscosity. Tung and Ting[11] have devised a singular-perturbation theory of vortex motion, from which they conclude that Eq. (14) applies to a diffusing vortex ring, provided c is taken as $2(\nu t)^{1/2}$. Presumably (c/b) could be calculated along the lines of Ref. 1 for a bell-shaped vorticity distribution. The choice $\delta/\beta = 0.063$, however, is acceptable for now. Refinements can be deferred to the future when more will be known about real core structures.

7. Theoretical Predictions

It was shown in Sec. 5 that three preferred modes of instability exist for any $\delta/\beta \lesssim 0.4$, each having a local maximum of α along the β-axis. According to Fig. 10, the symmetric mode S preferred under strong interaction in the case $\delta/\beta = 0.063$ lies at a $\beta_{max} = 0.73$. The other two preferred modes, S and A under weak interaction, consist of much shorter waves at a $\beta_{max} = 17$. The short waves are not observed in practice, although nothing in stability theory precludes their appearance. They amplify slightly faster, in fact, than the long waves. Obviously another criterion is operating to make a final selection among the three modes offered by stability theory.

Atmospheric turbulence probably makes the final selection. The Kolmogorov similarity theory implies that the amount of turbulent energy available to excite a mode of wavenumber k is proportional to $k^{-5/3}$. Turbulence drives the long waves associated with $\delta/\beta = 0.063$ a factor of $(0.73/17)^{-5/3}$ more energetically than it drives the short waves, and $(0.73/17)^{-5/3} = 190$. For values of δ/β as small as 0.063, the structure of atmospheric turbulence imposes an overwhelming bias in favor of the long waves, which are unstable only in the symmetric mode.

The β_{max} of that mode is 0.73 as already noted, and the other two dimensionless parameters follow from Figs. 11 and 12: $\alpha_{max} = 0.83$, and $\tan\theta_{max} = 1.11$. Those dimensionless quantities can be translated into a physical description of the mode arising from the combined action of instability and turbulent agitation:

1) The trailing vortices distort into symmetric waves of length $2\pi b/0.73 = 8.6b$. The wavelength is 6.8 times the span of the aircraft, since the vortex separation behind an elliptically loaded wing is $\pi/4$ times its span, as Spreiter and Sacks show in Ref. 1.

2) The instability grows by a factor e in a time $a^{-1} = 1.21(2\pi b^2/\Gamma_o)$, where $(2\pi b^2/\Gamma_o)$ is the time required for the vortices to move downward a distance b under their own induction. The circulation Γ_o can be expressed in terms of aircraft parameters by means of Eq. (10) of Ref. 1, with the result that $a^{-1} = 9.4(A_R/C_L)(b/V_o)$. Note that b denotes wingspan in Ref. 1, whereas here b stands for vortex separation. Compared with the process of vortex formation, the subsequent instability is very slow. The vortex sheet behind an elliptically loaded wing rolls up in a time $0.36(A_R/C_L)(b/V_o)$, according to Eq. (27) of Ref. 1. The time scale a^{-1} is 26 times longer.

3) The perturbed vortices are confined to fixed planes as shown in the upper illustration of Fig. 8. The planes are inclined to the horizontal at an angle $\theta = \tan^{-1}(1.11)$, which is 48°.

The predictions 1), 2), and 3) follow straight from the theory and involve no fitted constants. The very large wavelength of the preferred mode, namely $8.6b$, is perhaps surprising.

8. Comparison between Theory and Experiment

Although it can be seen quite regularly, the instability of trailing vortices rarely has been photographed. One piece of experimental evidence is Plate 2 of Ref. 3. Reference 2 contains several photographic sequences, one of which has been reproduced here as Fig. 1. Doubtless much more information will soon be available, but the evidence in Refs. 2 and 3 can be compared to the theoretical predictions as follows:

1) The wavelength in Fig. 1 is roughly $8b$. The wavelength in Plate 2 of Ref. 3 is about $9b$. Those estimates are very crude, so the striking agreement with the theoretically predicted wavelength of $8.6b$ may be partly fortuitous.

2) Figure 1 shows the vortex trail of a B-47 at cruising speed and altitude. The vortex spacing b was about 90 ft, and the aircraft speed V_o would have been about 720 fps. The ratio (C_L/A_R) for a cruising B-47 is about 0.055. Thus a^{-1} would have been about $9.4(90/720)(0.055)^{-1} = 21$ sec. That figure is of the right order-of-magnitude to explain the sequence of photographs in Fig. 1, though no really quantitative comparison is possible. The trailing vortices of Fig. 1 connected after 60 sec, at which time the linear instability would have grown by a factor $e^{60/21} = 17.4$, a reasonably large amplification. The time scale $a^{-1} = 21$ sec should apply approximately to the commercial jet transports as well as to a B-47. It is noteworthy that the time scale of the instability during approach to landing is not much different. (C_L/A_R) rises to about 0.18, V_o drops to about 220 fps, and a^{-1} remains unchanged as 21 sec.

3) There are no photographs that would permit even a rough evaluation of the angle θ. Figure 12 of Ref. 2, however, shows that the vortices do undergo sinusoidal displacements in the vertical direction.

As far as it goes, the comparison between theory and experiment is highly encouraging. It will be interesting to see how well the agreement persists as more quantitative data accumulate.

† In the preprint version of this paper, a slight arithmetical error was made in the computation leading to Eq. (13), and the coincidence between Eqs. (13) and (15) passed unnoticed. I am indebted to P. C. Parks for finding the error and pointing out the coincidence during his stay at the Langley Research Center.

References

[1] Spreiter, J. R. and Sacks, A. H., "The Rolling Up of the Trailing Vortex Sheet and Its Effect on the Downwash behind Wings," *Journal of the Aeronautical Sciences*, Vol. 18, No. 1, Jan. 1951, pp. 21–32.

[2] Smith, T. B. and Beesmer, K. M., "Contrail Studies of Jet Aircraft," ASTIA AD 217 188, April 1959, Meteorology Research Inc., Pasadena, Calif.
[3] Scorer, R. S., *Natural Aerodynamics*, Pergamon Press, New York, 1958, pp. 73–75.
[4] Batchelor, G. K., *An Introduction to Fluid Dynamics*, Cambridge University Press, Cambridge, England, 1967, p. 509.
[5] Moore, L., "The Spread of Vorticity in the Wake behind a Cylinder," *Proceedings of the Royal Society*, Ser. A, Vol. 127, 1930, pp. 590–612.
[6] Hama, F. R., "Progressive Deformation of a Curved Vortex Filament by its Own Induction," *The Physics of Fluids*, Vol. 5, No. 10, Oct. 1962, pp. 1156–1162.
[7] Thomson, Sir W., "Vibrations of a Columnar Vortex," *Mathematical and Physical Papers*, Vol. 4, Cambridge University Press, Cambridge, England, 1910, pp. 152–165.
[8] Jahnke, E. and Emde, F., *Tables of Functions*, 4th ed., Dover, New York, 1945, pp. 3–9.
[9] Watson, G. N., *Theory of Bessel Functions*, 2nd ed., Cambridge University Press, Cambridge, England, 1952, pp. 698–713.
[10] Lamb, Sir H., *Hydrodynamics*, 6th ed., Cambridge University Press, Cambridge, England, 1932, p. 241.
[11] Tung, C. and Ting, L., "Motion and Decay of a Vortex Ring," *The Physics of Fluids*, Vol. 10, No. 5, May 1967, pp. 901–910.

DECEMBER 1970 AIAA JOURNAL VOL. 8, NO. 12

Boundary-Layer Displacement and Leading Edge Bluntness Effects on Attached and Separated Laminar Boundary Layers in a Compression Corner. Part I: Theoretical Study

MICHAEL S. HOLDEN*
Cornell Aeronautical Laboratory, Inc., Buffalo, N.Y.

This paper describes a theoretical analysis of highly cooled attached and separated regions of shock wave-laminar boundary-layer interaction in the presence of strong streamwise pressure gradients generated by boundary-layer displacement effects at the leading edge. This method is an extension of an earlier analysis by Holden[1,12] to conditions where the inviscid flow cannot be described by simple isentropic flow relationships, and where the boundary-layer upstream of the main interaction is subjected to a strong pressure gradient. The analysis is compared with measurements described in Part II of the study. For strong leading edge displacement effects ($\bar{\chi}_L > 1$), the analysis predicts that highly cooled boundary layers in hypersonic flow will be supercritical; a supercritical-subcritical jump is therefore required to join the solution to the subcritical viscous layer at separation. An examination of the experimental measurements indicates that the supercritical-subcritical jump does not reflect a sudden and basic change in the flow mechanics of separation, but is an approximation necessary because the conventional boundary-layer equations cannot adequately describe the viscous interaction process leading to separation. For some high Mach number, low Reynolds number conditions, we were unable to obtain a unique solution, without recourse to experimental data, by locating a critical point in the throat region of the flow. As in the separated region, there is serious question whether the conventional boundary-layer equations can be used to adequately describe the mechanism of boundary-layer reattachment in these flows.

Nomenclature

a = speed of sound
C_F = the skin-friction coefficient
C_H = the surface heat-transfer coefficient
C_P, C_V = specific heats of the gas at constant pressure and at constant volume, respectively
C = the constant of proportionality in the linear viscosity-temperature relation $\mu/\mu_\infty = CT/T_\infty$
C_* = $[\mu(T^*)/\mu(T_\infty)]T_\infty/T_*$
D_N = drag of the blunt leading edge
h = static enthalpy
h_S, H = total enthalpy
k = leading edge drag coefficient $D_N/\frac{1}{2}\rho_\infty U_\infty{}^2 l$
L = reference length
M = Mach number
p = pressure
Pr = Prandtl number
q = local surface heat-transfer rate
Re_x = Reynolds number $\rho ux/\mu$
S = enthalpy function $h_e/h_{S_e} - 1$
S_W = $h_W/h_{S_e} - 1$
t = leading edge thickness
U, V = the velocity components parallel to the x and y axes, respectively
x, y = coordinates parallel to and normal to the surface, respectively
γ = specific heat ratio
δ, δ^* = boundary-layer thickness and displacement thickness, respectively
ϵ = $\gamma - 1/\gamma + 1$
θ = wedge angle
Θ = local angle between x axis and streamline at the edge of the boundary layer
κ_ϵ = a parameter controlling inviscid tip bluntness effect, $\kappa_\epsilon = M^3 kt/x$
μ = dynamic viscosity

Presented as Paper 68-68 at the AIAA 6th Aerospace Sciences Meeting, New York, January 22–24, 1968; submitted January 29, 1969; revision received April 14, 1970. This research was sponsored by the Aerospace Research Laboratories, Office of Aerospace Research, United States Air Force under Contract F33615-67-C-1298.

* Principal Aerodynamicist, Aerodynamic Research Department. Associate AIAA.